ACS APPLIED MATERIALS & INTERFACES

Research Article

www.acsami.org

Self-Reactivated Mesostructured Ca−Al−O Composite for Enhanced High-Temperature CO_2 Capture and Carbonation/Calcination Cycles Performance

Po-hsueh Chang, Wei-Chen Huang, Tai-Jung Lee, Yen-Po Chang, and San-Yuan Chen*

Department of Materials Science and Engineering, National Chiao Tung University,Hsinchu 300, Taiwan

Supporting Information

sample code[a]	Ca/Al	Ca^{2+} (mole)	Al^{3+} (mole)	CO_2, capture (g-CO_2/g-sorbent, %) 1 cycles	CO_2, capture (g-CO_2/g-sorbent, %) 20 cycles[c]	specific surface area[b] (m^2 g^{-1}) M-CAO	specific surface area[b] (m^2 g^{-1}) 20 cycles[c]	pore volume (cm^3 g^{-1}) M-CAO	pore volume (cm^3 g^{-1}) 20 cycles[c]	pore diameter[d] (nm) M-CAO	pore diameter[d] (nm) 20 cycles[c]
MA-matrix						277		0.76		12.4	
M-CAO-1	1:1	0.49	0.51	1.2	1.5	201		0.55		11.6	
M-CAO-3	3:1	0.75	0.25	22.4	38.7	171		0.49		10.7	
M-CAO-5	5:1	0.82	0.18	36.7	47.2	132	139	0.37	0.43	7.9	8.2
M-CAO-8	8:1	0.89	0.11	46.6	33.4	69	41	0.17	0.12	5.4	4.3

[a]Calcined at 600 °C for 3 h. [b]BET specific surface area. [c]After 20 cycles of carbonation/calcination. [d]BJH desorption average pore diameter.

ABSTRACT: In this study, highly efficient high-temperature CO_2 sorbents of calcium aluminate (Ca−Al−O) mesostructured composite were synthesized using presynthesized mesoporous alumina (MA) as a porous matrix to react with calcium nitrate through a microwave-assisted process. Upon annealing at 600 °C, a highly stable mesoporous structure composed of poorly crystalline $Ca_{12}Al_{14}O_{33}$ phase and the CaO matrix was obtained. The Ca−Al−O mesostructured sorbents with a Ca^{2+}/Al^{3+} ratio of 5:1 exhibit an enhanced increasing CO_2 absorption kinetics in the CO_2 capture capacity from 37.2 wt % to 48.3 wt % without apparent degradation with increasing carbonation/calcination cycling up to 50 at 700 °C due to the strong self-reactivation effect of the mesoporous Ca−Al−O microstructure. Remarkable improvements in the CaO-$CaCO_3$ conversion attained from the mesostructured Ca−Al−O composite can be explained using the concept combined with available mesoporous structure and $Ca_{12}Al_{14}O_{33}$ phase content. However, a high Ca^{2+}/Al^{3+} =8:1 Ca−Al−O composite causes degradation because the pores become blocked and partial sintering induces CaO agglomeration.

KEYWORDS: *Ca−Al−O mesoporous, carbon dioxide capture, carbonation/calcination, microwave-assisted*

1. INTRODUCTION

CO_2 generated from power plants has been recognized as one of the major contributors to global CO_2 emissions. As a promising way to address global warming and climate change, the capture and storage of CO_2 from fossil fuels has gained increasing interest in recent years.[1] Several material and approaches systems can be used to capture CO_2, including liquid-phase solvents,[2,3] membranes,[4,5] molecular sieves,[6,7] solid sorbents,[8,9] supercritical CO_2,[10,11] and electrochemical CO_2 capture.[12−14] Although calcium oxide (CaO) sorbents have received much attention because of their remarkable CO_2 capture capacity at high temperature (700 °C) and the wide availability of their components in natural minerals (obtained by simple calcination treatment), the sorbents exhibit poor stability over multiple carbonation/calcination cycles.[9,15,16] To date, many investigations have been conducted to improve the sintering resistance of CaO-based sorbents, which have been comprehensively summarized in recent reviews.[17−19] The addition of supports or incorporation of active CaO into an inert solid matrix has been a very promising method in this respect because the inert supports enabled to separate CaO particles and prevent or delay them from sintering at high temperature.[20] Aluminum compounds (alumina and calcium aluminate) are the most widely used support materials because of their relatively high Tammann temperature (891 °C) and high mechanical strength.[19] For example, $Ca_{12}Al_{14}O_{33}$ (mayenite) has been widely used as a stabilizer and sintering-resistant material to prevent performance degradation during carbonation/calcination cycling. Li et al.[21,22] reported that $Ca_{12}Al_{14}O_{33}$-stabilized CaO sorbents with a CaO/$Ca_{12}Al_{14}O_{33}$ mass ratio of 75/25 possessed a high CO_2 capture capacity of 0.41 g of CO_2/g of sorbent over 50 carbonation/calcination cycles. Following the same technique, Martavaltzi et al. improved the capture performance of CaO-$Ca_{12}Al_{14}O_{33}$ sorbents by using the calcium acetate precursor and the sorbent containing 85 wt % CaO exhibited a high CO_2 capture capacity over 45 cycles of carbonation/calcination at 690 °C.[23,24] Xu et al.[25] reported a series of CaO-based sorbents consisting of active CaO and inert $Ca_9Al_6O_{18}$ by a sol−gel method with various calcium precursors and found that the sorbent with a CaO content of 90 wt % derived from calcium lactate displayed the best performance for CO_2 capture capacity

Received: January 2, 2015
Accepted: March 2, 2015
Published: March 2, 2015

DOI: 10.1021/acsami.5b00033
ACS Appl. Mater. Interfaces 2015, 7, 6172−6179

Table 1. Nitrogen Adsorption/Desorption Isotherms and Characteristics of the Sorbents with Different Ca^{2+}/Al^{3+} Molar Ratios Synthesized at 80 °C for 1 h

				CO_2, capture (g-CO_2/g-sorbent, %)		specific surface area[b] (m^2 g^{-1})		pore volume (cm^3 g^{-1})		pore diameter[d] (nm)	
sample code[a]	Ca/Al	Ca^{2+} (mole)	Al^{3+} (mole)	1 cycles	20 cycles[c]	M-CAO	20 cycles[c]	M-CAO	20 cycles[c]	M-CAO	20 cycles[c]
MA-matrix						277		0.76		12.4	
M-CAO-1	1:1	0.49	0.51	1.2	1.5	201		0.55		11.6	
M-CAO-3	3:1	0.75	0.25	22.4	38.7	171		0.49		10.7	
M-CAO-5	5:1	0.82	0.18	36.7	47.2	132	139	0.37	0.43	7.9	8.2
M-CAO-8	8:1	0.89	0.11	46.6	33.4	69	41	0.17	0.12	5.4	4.3

[a]Calcined at 600 °C for 3 h. [b]BET specific surface area. [c]After 20 cycles of carbonation/calcination. [d]BJH desorption average pore diameter.

of 0.59 g of CO_2/g of sorbent at the 35th carbonation/calcination cycle. However, the CO_2 capture capacity and degradation behavior of CaO-$Ca_{12}Al_{14}O_{33}$ sorbents is strongly dependent on the distribution of the $Ca_{12}Al_{14}O_{33}$ sorbent in the CaO-based matrix. Zhang et al. reported that CaO−Al_2O_3 sorbents with high specific surface areas can be synthesized by calcining a mixture of aluminum and calcium precursors below 800 °C.[26] Recently, Florin et al.[27] synthesized $Ca_{12}Al_{14}O_{33}$-stabilized CaO-based sorbents by coprecipitating an aqueous slurry of $Ca(OH)_2$ and $Al(NO_3)_3$ with CO_2, which was bubbled through the slurry, followed by drying and calcination. Although, a high CO_2 capture capacity and stable carbonation/calcination cycles can be achieved, a porous Ca−Al−O-based composite structure which provides relatively rapid CO_2 absorption kinetics and conversion is very important for enhancing stable carbonation/calcination performance at high temperatures for CO_2 capture.

In recent years, microwave-enhanced chemistry has become increasingly important because through the techniques, the inherent properties of liquids, solids, and their mixtures can be utilized in situ to promote the rapid synthesis of numerous ceramic oxides, hydroxylated phases, and porous materials.[28] Furthermore, the microwave technique has been widely applied for the synthesis of mesoporous materials (such as MCM-41 and SBA-15)[29] because it offers many advantages such as homogeneous and simultaneous heating to enhance rapid nucleation and growth so that a uniform porous spherical structure was formed to facilitate CO_2 diffusion and reaction with inner sorbent effectively, resulting in a significant improvement in initial CO_2 carbonation capacity and kinetic rate. Therefore, in this study, we proposed this new method to synthesize mesoporous calcium aluminate (Ca−Al−O) structures for providing relatively rapid CO_2 capture kinetics, high CO_2 conversion, and stable carbonation/calcination performance at high temperature using microwave-assisted synthesis. The structural and morphological evolution of calcium aluminate mesostructured sorbents with various Ca^{2+}/Al^{3+} molar ratios were characterized by powder X-ray diffraction (PXRD), N_2 adsorption/desorption isotherms, scanning electron microscopy (SEM), and transmission electron microscopy (TEM). The possible formation mechanism of the calcium aluminate mesostructured compounds was also investigated. A detailed study on the high-temperature CO_2 capture behavior and multiple carbonation/calcination cycles of the Ca-rich mesostructured oxide sorbents using a thermogravimetric analyzer (TGA) was also performed.

2. EXPERIMENTAL SECTION

2.1. Sample Preparation and Characterization of Mesoporous Ca/Al Nanocomposite Materials. Highly ordered mesoporous alumina (MA) with high thermal stability can be synthesized. In a typical preparation, triblock copolymer $HO(CH_2CH_2O)_{20}(CH_2CH(CH_3)O)_{70}-(CH_2CH_2O)_2OH$ (2 g; Sigma−Aldrich, M_n = 5800, Pluronic P123) was dissolved in dehydrated alcohol (20 mL; Sigma−Aldrich, 99.8%) and stirred for 4 h at room temperature. In another solution, aluminum isopropoxide (AIP, 20 mmol; Sigma−Aldrich, 98+ wt %,) was dissolved in nitric acid (3.2 mL; J.T. Baker,70 wt %) and dehydrated alcohol (10 mL). After the appropriate amount of the AIP solution was slowly added to the surfactant solution, the mixed solution was vigorously stirred for 5 h and then transferred to an oven to evaporate the solvent at 60 °C for 3 days. The resulting powder was calcined at 700 °C for 4 h at a heating rate of 5 °C min^{-1} in an air flow and then cooled in a furnace to ambient temperature to yield mesoporous Al_2O_3 (denoted as MA). The synthesized MA and calcium nitrate were used as starting materials. These materials, with Ca^{2+}/Al^{3+} molar ratios of 1:1, 3:1, 5:1, and 8:1, were suspended in 100 mL of a dehydrated alcohol solution at room temperature. The solutions were then transferred to tetrafluoromethyl (TFM) reactors. The reactors containing the suspensions were sealed and then placed on a turntable tube for uniform heating by a microwave-accelerated reaction system (model MARSTM, CEM Corporation, Matthews, NC, USA). The suspensions in the TFM vessels were heated to 50 and 80 °C for 1 h in a microwave oven with 1200 W of power. The precipitates suspended in the solutions were rapidly dried at 50 °C in an oven overnight to remove the solvent. Finally, the resulting powders were calcined at 600 °C for 3 h at a heating rate of 2 °C min^{-1} in an air flow to yield powders with Ca^{2+}/Al^{3+} molar ratios of 1:1, 3:1, 5:1, and 8:1, denoted M-CAO-l, M-CAO-3, M-CAO-5, and M-CAO-8, respectively.

The powders were characterized by XRD measurements (MAC Science MXP18AHF XRD, with CuKa radiation source, λ = 1.5418 A). The existing crystalline phases in the powders were identified based on comparisons with JCPDS diffraction data files. The specific surface area (BET) and pore size distribution were calculated using an ASAP 2020 instrument and nitrogen adsorption isotherms at −196 °C. All samples were degassed under vacuum at 200 °C for 2 h prior to the measurements. Fourier transform infrared spectroscopy (FTIR) was recorded on a PerkinElmer spectrum 100 spectrometer by using KBr pellets. SEM images of the samples were collected with a JEOL-6700 field-emission electron microscope at an accelerating voltage of 15 kV. TEM micrographs and electron diffraction patterns were recorded with a JEOL JEM-2100F electron microscope. Samples for TEM measurements were embedded in resin and ultramicrotomed into slices with thicknesses of approximately 50 nm. The samples were digested with mixed acids, and their Ca^{2+}/Al^{3+} molar ratios were determined by ICP-AES (Jarrell-Ash, ICAP-9000).

2.2. CO_2 Capture Analysis. Using a thermal gravimetric analyzer (TGA,TA Instrument Q500), the weight changes of the M-CAO CO_2 sorbents synthesized with different Ca^{2+}/Al^{3+} molar ratios during carbonation and calcination were measured. Multiple-cycle testing was performed by carbonating the samples in pure CO_2 gas (99.99%) at

DOI: 10.1021/acsami.5b00033
ACS Appl. Mater. Interfaces 2015, 7, 6172−6179

600 °C for 5 min and calcining the samples in 100% N_2 gas at 700 °C for 8 min at a flow rate of 60 mL/min. The cycles were repeated 20 times to determine the CO_2 capture and thermal stability of the M-CAO sorbents.

3. RESULTS AND DISCUSSION

3.1. Characterization of Mesoporous Ca−Al Composite Sorbents. The mesoporous calcium aluminate nanocomposites with different Ca^{2+}/Al^{3+} molar ratios were synthesized by reacting mesoporous Al_2O_3 (MA) with a controlled concentration of calcium via the microwave-assisted process at 80 °C with calcination at 600 °C. Table 1 shows that the actual Ca^{2+}/Al^{3+} molar ratios of M-CAO-l, M-CAO-3, M-CAO-5, and M-CAO-8 were measured to be 0.96, 2.83, 4.88, and 8.09, respectively, by ICP-AES. Figure 1 shows the small-angle XRD pattern of mesoporous Al_2O_3, in which the characteristic reflections of the *P6mm* hexagonal mesostructure at $2\theta = 0.77°$ (MA) are displayed and the corresponding *d*-spacing is indexed to $d_{100} = 11.5$ nm. With an increase in the Ca^{2+}/Al^{3+} molar ratio, the small-angle XRD patterns of the composites samples (M-CAO-l, M-CAO-3, M-CAO-5, and M-CAO-8) display a single broad diffraction peak at $2\theta = 0.80$, 0.82, 1.06, and 1.32°, corresponding to a decrease in pore size, as demonstrated by the decrease in *d*-spacing from 11 to 6.69 nm. However, the low intensity and broadness of the diffraction peak in the small-angle region indicate a wormhole framework, which reveals that Ca^{2+} loading may result in the amorphous structure of the composites. The existence of this small-angle diffraction peak also indicates that the sorbents still retained the mesostructure throughout the calcination process.[30] At a Ca^{2+}/Al^{3+} ratio of 8:1, the mesostructure began to disappear, indicating that the incorporation of additional Ca^{2+} caused a decrease in *d*-spacing along the *a*-axis. The transmission electron microscopy (TEM) images of the MA, M-CAO-1, M-CAO-3, and M-CAO-5 samples are further shown in Figure 2. The morphology of the MA clearly shows a highly ordered array of pores. For the M-CAO-1, M-CAO-3, and M-CAO-5 samples, the porosity was observed to become more random and to decrease with an increase in the Ca^{2+}/Al^{3+} molar ratio, which is consistent with the BET data reported in Table 1. In addition, the nitrogen adsorption−desorption isotherms of mesoporous Al_2O_3 (MA) and M-CAO-5 samples are shown in Figure S1 in the Supporting Information. The hysteresis loop of MA sample displayed type H1 characteristic and the steepness of the capillary condensation step indicated the uniformity of the mesopores. In contrast, the M-CAO-5 sample showed a hysteresis loop of type H2, which is typical for wormhole framework structures.[31,32] These results indicate that by increasing the Ca^{2+} ion content, the specific surface area of the M-CAO powders decreased from 201 to 69 m^2/g. For M-CAO-8 in particular, the pores were difficultly identified from the TEM images, which suggests that during the microwave-assisted synthesis, not all of the Ca^{2+} ions from the $Ca(NO_3)_2$ phase completely reacted with mesoporous Al_2O_3 to form a Ca−O−Al mesostructure and that some CaO particles could be precipitated to block the pores.

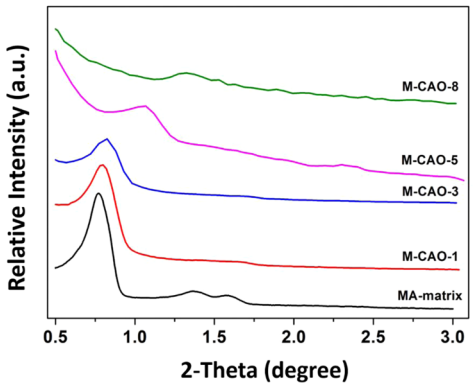

Figure 1. Small-angle XRD patterns of sorbents with different Ca^{2+}/Al^{3+} molar ratios synthesized at 80 °C for 1 h and calcined at 600 °C.

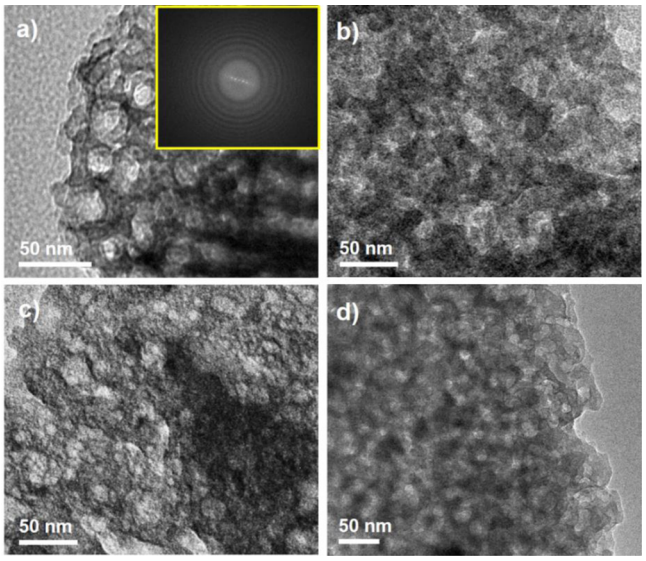

Figure 2. TEM images of (a) MA matrix, with lattice fringes shown in the boxed area, and sorbents with molar ratios of (b) M-CAO-1, (c) M-CAO-3, and (d) M-CAO-5.

Figure 3a shows the large-angle XRD (LA-XRD) patterns of the as-synthesized calcium aluminate nanocomposite powders, which were synthesized at 80 °C for 1 h. The XRD pattern of the MA sample shows only the boehmite phase structure. However, because the MA reacted with Ca^{2+} ions under the microwave thermal treatment, the M-CAO-1 sample exhibited an amorphous matrix, indicating that the formation of hydrated $Ca-Al_2O_3$ possibly occurred between mesoporous Al_2O_3 and calcium species during microwave treatment. As the Ca^{2+} ion content of the M-CAO-3 sample increased, the sample displayed a poorly crystalline $Ca(OH)_2$ phase. Upon increasing the Ca^{2+}/Al^{3+} molar ratio to 5, the $Ca(OH)_2$ phase could be clearly detected from the XRD pattern, revealing that the $Ca(OH)_2$ phase precipitated in the Ca-containing MA matrix. When calcined at 700 °C, the MA sample displayed three broad peaks due to reflections from the (311), (400), and (440) planes, which correspond to those of crystalline γ-Al_2O_3 (JCPDS No. 29−0063), indicating a crystalline γ-Al_2O_3 framework. The large-angle XRD (LA-XRD) patterns of the mesoporous nanocomposites shown in Figure 3b further indicate that the $Ca_{12}Al_{14}O_{33}$ phase (JCPDS No. 70−2144) could be formed in the M-CAO sorbents. When the Ca^{2+}/Al^{3+} molar ratio was fixed to approximately 1, only the $Ca_{12}Al_{14}O_{33}$ phase was identified in the M-CAO-1 sample. The peaks also indicate that mesoporous Ca-containing aluminate nanostructures could be formed by calcination at 600 °C in this compound. For the M-CAO-3, M-CAO-5, and M-CAO-8 samples, the XRD patterns indicate the simultaneous formation

DOI: 10.1021/acsami.5b00033
ACS Appl. Mater. Interfaces 2015, 7, 6172−6179

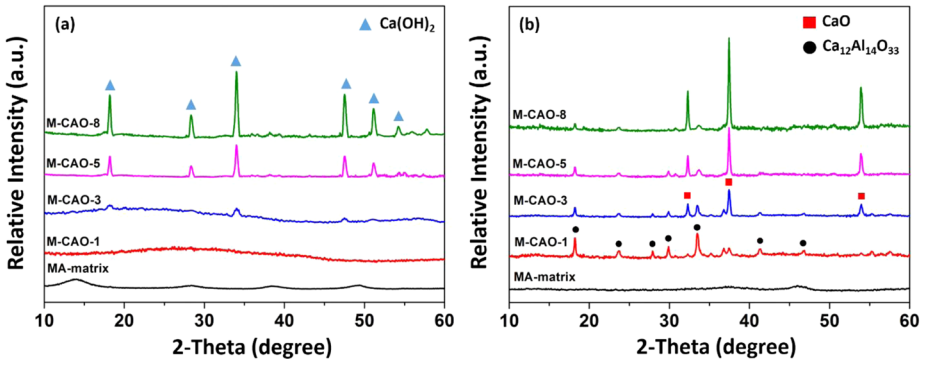

Figure 3. Large-angle XRD patterns of (a) the as-synthesized at 80 °C for 1 h and (b) 600 °C calcined powders.

of a CaO phase and a $Ca_{12}Al_{14}O_{33}$ phase (the latter indicated by weak peaks); the patterns also show that the peak intensity of the $Ca_{12}Al_{14}O_{33}$ phase decreased with an increase in the Ca^{2+}/Al^{3+} molar ratio. It is implied that the extra Ca^{2+} species that did not react with the mesoporous Al_2O_3 could have been transferred to form calcium oxide after calcination at 600 °C.

This interaction between MA and Ca^{2+} ions during the microwave thermal treatment can be further illustrated by using FTIR spectra for the as-synthesized and calcined samples (M-CAO-3) in Figure 4a, b. For the microwave-assisted treatment,

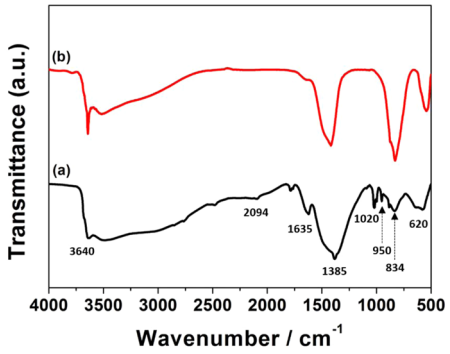

Figure 4. FTIR spectra of the M-CAO-3 sample (a) as-synthesized and (b) calcined at 600 °C.

the pair of bands at 950 and 1020 cm^{-1} may be associated with the characteristic vibrations of the Al−OH bonding. In Figure 4a, the O−H stretching vibration bands (Ca/Al−OH) can be clearly observed at 834 and 3640 cm^{-1}. The broad peaks at 620 and 2094 cm^{-1} could be assigned to stretching and bending modes of AlO−(OH).[33] The intense bands at 1385 and 1635 cm^{-1} are due to the vibration of H_2O molecules that took part in hydrogen bonding with the Al_2O_3 surface.[34] It is implied that a possible hydrated formation of Ca−Al_2O_3 occurred between mesoporous Al_2O_3 and calcium species during microwave treatment. After calcination at 600 °C, a broad band centered at 3510 cm^{-1} and a sharp peak at 3640 cm^{-1} (Ca−OH and Al−OH bond) was observed (Figure 4b). In addition, the bands appearing in the 500−900 cm^{-1} low-frequency region were assigned to the symmetric and asymmetric stretching of the −Al−O−Ca and Ca−O bonds. Therefore, it was demonstrated that the formation of Ca−Al−O linkages could be promoted by using the microwave-assisted treatment process. The FTIR analysis of the M-CAO sample is consistent with the XRD results.

To confirm the formation temperature of the $Ca_{12}Al_{14}O_{33}$ phase, we treated samples of the M-CAO-1 composite at various temperatures. The XRD pattern in Figure S2 in the Supporting Information indicates that the $Ca_{12}Al_{14}O_{33}$ phase began to form at 500 °C although the peaks show broadening. It has been reported that the $Ca_{12}Al_{14}O_{33}$ phase is usually formed after calcination above 800 °C.[35] However, in this work, this phase weakly appeared after calcination at 500 °C and was clearly detected after calcination at 600 °C (Figure S2 in the Supporting Information). This discrepancy in the formation temperature of the $Ca_{12}Al_{14}O_{33}$ phase may be related to microwave heating because microwave radiation can directly interact with the dipoles of molecules, resulting in accelerated reactions between Ca^{2+} ions and mesoporous Al_2O_3. During microwave heating, the Ca^{2+} ions were evenly distributed throughout the porous structure of the composites to induce a stronger affinity of the Ca^{2+} ions toward the highly active mesoporous Al_2O_3 matrix;[36] thus, the reactions between Ca^{2+} and Al−O species could occur at lower temperatures to form mesoporous calcium-containing aluminate composites. However, during calcination at 400 °C, the product showed a high sticky-like melting form; thus, we could not measure the crystallinity using XRD.

3.2. Ca^{2+}/Al^{3+} Molar Ratio on CO_2 Capture and Carbonation/Calcination Behavior. The CO_2 capture kinetics of M-CAO sorbents with different Ca^{2+}/Al^{3+} molar ratios at 600 °C are illustrated in Figure S3a in the Supporting Information. It was observed that, except for the M-CAO-1 sample, the M-CAO powders exhibited a high CO_2 capture rate, which is possibly related to the CaO content and mesostructure of M-CAOs particle generated by microwave-assisted synthesis. Two distinct kinetic regimes are observed during CO_2 capture: fast capture occurs over the first 5 min because of chemical-reaction-controlled carbonation (chemical absorption), whereas at a later stage, a continuous but much slower increment in sample weight is observed, which is controlled by the diffusion (physical adsorption) of CO_2 gas through the mesostructure. Comparing the CO2 capture kinetics of M-CAO-3 and M-CAO-8 reveals that the weight increase of the former sample in the diffusion-controlled region is higher than that of the latter sample because CO_2 capture through physical adsorption is mainly dominated by the mesoporous structure. However, the CO_2 absorption kinetics are faster for the M-CAO-8 sorbent than for either the M-CAO-3 or M-CAO-5, as shown in Figure S3b in the Supporting Information because a large amount of CaO was accumulated on the MA surface to cause rapid CO_2 capture. This finding is in good agreement with the BET results (Table 1), which show

DOI: 10.1021/acsami.5b00033
ACS Appl. Mater. Interfaces 2015, 7, 6172−6179

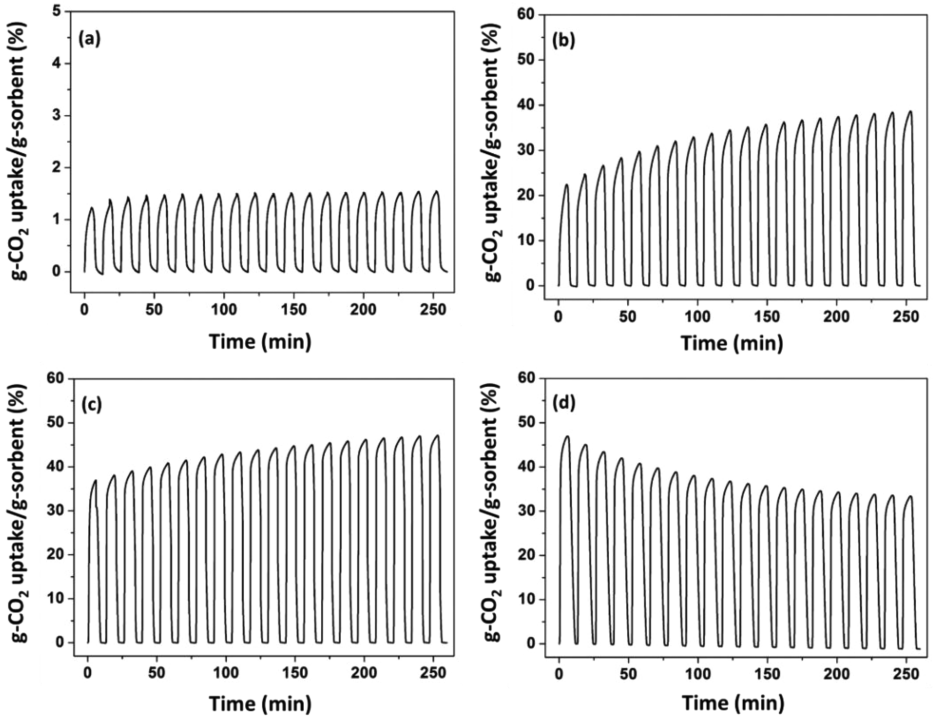

Figure 5. Long-term stability of the CO_2-uptake efficiency of sorbents with molar ratios of (a) M-CAO-1, (b) M-CAO-3, (c) M-CAO-5, and (d) M-CAO-8 during cycling at 100% CO_2 for 5 min (carbonation) at 600 °C and 100% N_2 for 8 min (calcination) at 700 °C.

that increasing the CaO concentration leads to a decrease in the specific surface area and pore size of the M-CAO-8 sample.

In addition to an adequate CO_2 capture capacity, to have further applications under actual operating conditions, sorbents should exhibit high stability during high-temperature carbonation/calcination cycling, which might be the most critical factor that determines the value of a sorbent material. The long-term carbonation/calcination cycling of the sorbents was performed under carbonation in pure CO_2 gas at 600 °C for 5 min and calcination in N_2 gas at 700 °C for 8 min. The results obtained for the M-CAO-1, M-CAO-3, M-CAO-5, and M-CAO-8 samples are shown in Figure 5a–d. After 20 cycles, except for that of the M-CAO-8 sorbent, the capture capacity of the sorbents was entirely maintained and even exhibited an increasing trend in weight change over the 20 cycles. In contrast, the CO_2 capture capacity of the M-CAO-8 sorbent decreased from 46.6 wt % to 33.4 wt % over the 20 cycles. This decay in the CO_2 capture capacity may be attributed to the fact that more CaO particles were distributed and accumulated on the surface of the mesostructured material, thus making CO_2 diffusion or penetration into the inner pores more difficult. Moreover, the large number of CaO particles on the surface facilitated particle aggregation or sintering. Therefore, although the CO_2 capture capacity could be increased by applying a higher Ca^{2+}/Al^{3+} molar ratio, the ability to absorb CO_2 was greatly reduced during carbonation/calcination cycling. In contrast, although the maximum capture capacity of the M-CAO-5 sorbent was approximately 36.7 wt % over the first few cycles (lower than that of the M-CAO-8 sorbent), the CO_2 capture capacity of the sorbent continuously increased up to 47.2 wt % (an approximately 28.6% increase than the first-cycle CO_2 capture capacity) after 20 carbonation/calcination cycles. On a similar basis of CaO/$Ca_{12}Al_{14}O_{33}$ mass ratio of 75/25, our sorbent presented a higher CO_2 capture capacity of 0.52 g of CO_2/g of sorbent over 50 carbonation/calcination cycles compared to the value (0.41) reported by Li et al.,[22] which can be attributed to self-reactivated effect of this CaO-based mesoporous sorbents. On the other hand, although the $Ca_9Al_6O_{18}$–CaO sorbent with a CaO content of 90 wt % displayed the best performance for CO_2 capture capacity of 0.59 g of CO_2/g of sorbent.,[25] the M-CAO-5 sorbent provided relatively rapid CO_2 capture kinetics, highly CO_2 conversion and stable carbonation/calcination performance at high temperature. This might reveal that the CO_2 capture process is strongly affected by the mesoporous structure of the sorbents and distribution of the $Ca_{12}Al_{14}O_{33}$ phase because the $Ca_{12}Al_{14}O_{33}$ phase can inhibit the aggregation and partial sintering of CaO/$CaCO_3$ particles. For the M-CAO-3 and M-CAO-5 sorbents, the increase in CO_2 capture capacity with cycle number can likely be explained using a self-reactivation phenomenon proposed by Lysikov et al.[37] because the MA supporting matrix not only provides a porous structure but also acts as a physical barrier, like an ion-induced hard skeleton to maintain the mesostructure during carbonation/calcination cycling. As schematically illustrated in Figure 6, as the CO_2 was diffused into the internal region of the MA or $Ca_{12}Al_{14}O_{33}$ matrix during carbonation, the $Ca_{12}Al_{14}O_{33}$ matrix can be considered as a hard skeleton, which can keep the pore morphology from being destroyed by sintering. On the other hand, the CaO or $CaCO_3$ on the MA/$Ca_{12}Al_{14}O_{33}$ matrix can be considered as external soft skeleton so that it is easily altered during $CaCO_3$ formation and decomposition, resulting in changes in particle morphology. Based on the assumption, the CO_2 capture capacity is low during initial cycling, indicating that the inner region of pores is less reactive because of the slow ion diffusion required for carbonation. However, the subsequent carbonation/calcination cycling can induce a larger external skeleton and/or pore volume, leading to an increased number of exposed active sites and an acceleration of the carbonation rate. Therefore, the CO_2 capture capacity increases

DOI: 10.1021/acsami.5b00033
ACS Appl. Mater. Interfaces 2015, 7, 6172–6179

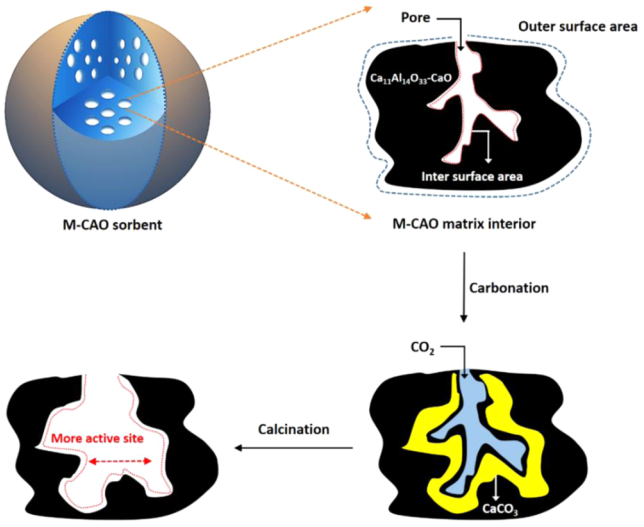

Figure 6. Morphology changes in the pore skeleton via self-reactivation during high-temperature carbonation/calcination cycling.

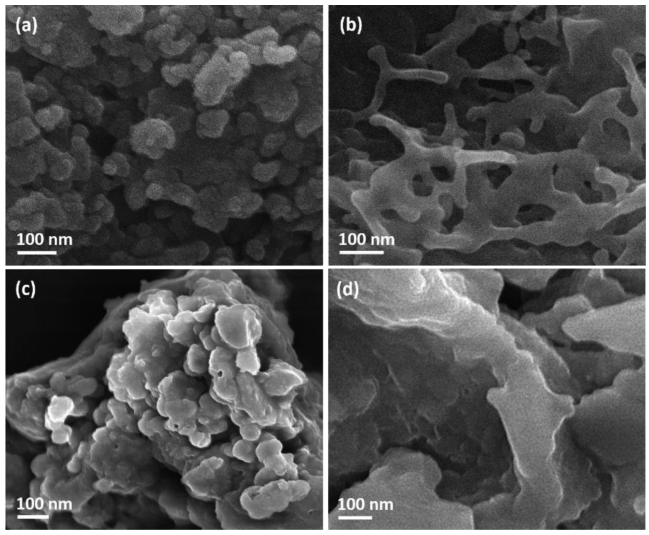

Figure 7. SEM images of sorbents with different Ca^{2+}/Al^{3+} molar ratios before and after 20 cycles of carbonation for 5 min at 600 °C and calcination for 8 min at 700 °C. M-CAO-5: (a) before and (b) after cycling. M-CAO-8: (c) before and (d) after cycling.

with cycle number as the external soft skeleton continues to grow, which could explain why the M-CAO-5 sorbent displayed a high CO_2 capture capacity over multiple carbonation/calcination cycles. At the same time, the $Ca_{12}Al_{14}O_{33}$ phase (in the black area) uniformly formed and dispersed within the MA matrix can inhibit aggregation and partial sintering between $CaO/CaCO_3$ particles, which can make more contribution to avoid the performance decay of CO_2 capture with cycles. However, with further cycling, the CO_2 capture capacity gradually reaches a maximum, i.e., a saturation level, which may be attributed to competition between the absorption reaction and bulk mass transfer. In contrast, as the porous structure disappears or becomes covered with CaO particles, such as in the M-CAO-8 sorbent, the effect of self-reactivation is inhibited and CaO partial sintering or aggregation is easily formed; thus, in this study, a decrease in CO_2 capture with carbonation/calcination cycling was observed. Therefore, although the M-CAO-5 sorbent displayed slower absorption kinetics than the M-CAO-8 sorbent as shown in Figure S3b in the Supporting Information, it can reach a maximum CO_2 capture capacity without apparent performance degradation. This phenomenon can be further evidenced from the microstructure as shown in Figure 7. A scanning electron microscope (SEM) image of the calcined M-CAO-5 sorbent in Figure 7a revealed that partial aggregation of the CaO and/or CaO-$Ca_{11}Al_{14}O_{33}$ particles may occur but after 20 cycles of calcination/carbonation, no large agglomerates or lumps were observed as indicated in Figure 7b; this finding indicates that the structure still presented a loose and porous structure, which further supports the above-mentioned discussion. On the other hand, the SEM images of the calcined M-CAO-8 sorbent displayed larger particles with an irregular structure stacked outside of the MA support, as shown in Figure 7c. After 20 cycles at 700 °C, the agglomeration and partial sintering of the CaO particles were clearly observed, as shown in Figure 7d; this process largely reduced the number of active sites for CO_2 capture, thus decreasing the capacity during later cycles, in good agreement with both the XRD (Figure 3) and BET specific surface area (Table 1) results.

3.3. $Ca_{12}Al_{14}O_{33}$ Content and Pore Volume on CO_2 Capture and Carbonation/Calcination Behavior. The CO_2 capture performance of the sorbents is not only dominated by the CaO but also affected by the $Ca_{12}Al_{14}O_{33}$ phase content, which would vary with phase and structure evolution during microwave-assisted synthesis. To further investigate the $Ca_{12}Al_{14}O_{33}$ phase and mesoporous structure on the CO_2 capture and conversion of M-CAO-5 sorbent, we subjected the M-CAO-5 to the microwave process at 50 and 80 °C. The XRD in Figure 8 showed that a major CaO phase

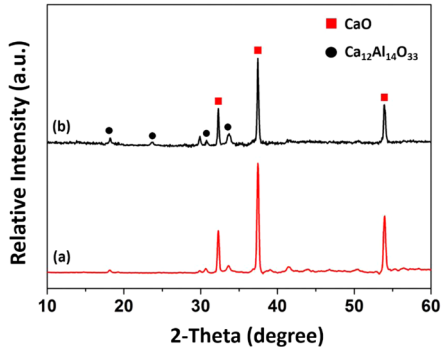

Figure 8. Large-angle XRD patterns of M-CAO-5 sorbents synthesized at different reaction temperatures and calcined at 600 °C: (a) 50 °C and (b) 80 °C.

accompanied by a minor $Ca_{12}Al_{14}O_{33}$ phase was detected in the M-CAO-5-50 sample (heated at 50 °C) as compared to that of M-CAO-5-80 sample (heated at 80 °C), indicating that the formation of $Ca_{12}Al_{14}O_{33}$ can be promoted during microwave-assisted processing due to tight Ca−Al bonding in the mesoporous Ca−Al−O structure.

The carbonation/calcination cycling performance of the sorbents was further tested up to 50 cycles to compare the long-term CO_2 capture behavior of M-CAO-5−50 with M-CAO-5−80 sorbent as previously described. Figure 9(a) showed that the M-CAO-5−50 sorbent displayed a higher initial CO_2 capture capacity than the M-CAO-5−80 sorbent but the carbonation/calcination multiple cycling test showed that the latter exhibited a significantly higher rate of CO_2 capture

DOI: 10.1021/acsami.5b00033
ACS Appl. Mater. Interfaces 2015, 7, 6172−6179

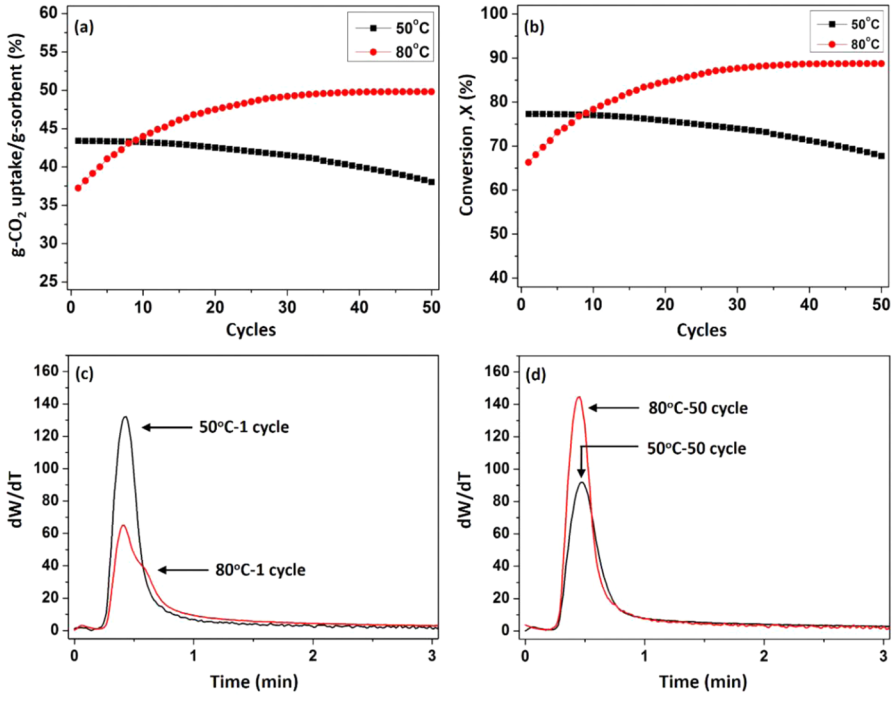

Figure 9. (a) Long-term stability of M-CAO-5 sorbents synthesized at 50 and 80 °C. (b) Carbonation conversions during CO_2 cycles. The sorbents were calcined at 600 °C and cycled through 5 min of carbonation and 8 min of calcination at 700 °C. CO_2 capture rate at (c) first and (d) 50th cycling of M-CAO-5 synthesized at 50 and 80 °C.

and greater CO_2 capture efficiency without apparent degradation. Figure S4 further demonstrated the M-CAO-5-80 sorbents exhibited excellent long-term stable carbonation/calcination cycling performance up to 200 cycles. This indicates that a high microwave reaction temperature can enhance the distribution of Ca ions to prevent CaO particles from aggregating on the MA surface and increase the BET specific surface area and pore volume from 113 to 132 m^2/g and 0.31 to 0.37 cm^3/g for M-CAO-5-50 and M-CAO-5−80 sorbents, respectively.

In addition, the carbon dioxide conversion of M-CAO-5 sorbent was further evaluated in Figure 9b for the first and 50th cycles. Although the initial CO_2 conversion in M-CAO-5-50 is higher than that in M-CAO-5-80 sorbent, the CO_2 conversion was much reduced at 50th cycling in the former sample (67.7%) compared to the latter sorbent (88.7%). Similar phenomenon was also observed in the CO_2 capture rate as demonstrated in Figure 9c, d. The M-CAO-5-50 sorbent exhibited a higher CO_2 capture rate at initial cycling, as shown in Figure 9c, but after 50 cycles, a higher CO_2 capture rate was observed in the M-CAO-5-80 sorbent because of the larger specific surface area and self-reactivation effect, as demonstrated in Figure 9d. The change in the CO_2 capture rate and conversion can be explained using the compromising concept combined with available specific surface area and $Ca_{12}Al_{14}O_{33}$ phase content. The results again demonstrated that the CaO distribution and reaction temperature in microwave process play important roles in the high-temperature CO_2 capture performance of CO_2 sorbents.

CONCLUSION

A highly stable high-temperature CO_2 sorbent of mesoporous Ca−Al−O composite material was successfully synthesized by a microwave-assisted process. The MA supporting material can effectively prevent the porous structure from being destroyed by the aggregation of CaO particles and enhance the CO_2 capture capacity. The M-CAO-3 and M-CAO-5 sorbents showed enhanced CO_2 capture capacity and CO_2 conversion efficiency due to self-activated reaction occurring in this mesoporous structure, leading to more exposed active sites and an accelerated carbonation rate. However, partial sintering of CaO could be observed on sorbents with high Ca^{2+}/Al^{3+} molar ratios because the pores were blocked with CaO aggregation. In comparison with other high-temperature CO_2 sorbents, these developed mesoporous Ca−Al−O composite provide both high CO_2 capture capacity and excellent thermal stability during the carbonation/calcination reaction. These promising results suggest that this newly developed CO_2 sorbent may have potential applications for sorption-enhanced steam methane reforming for hydrogen production and energy storage systems in chemical heat pumps.

ASSOCIATED CONTENT

Supporting Information

Additional figures (PDF). This material is available free of charge via the Internet at http://pubs.acs.org.

AUTHOR INFORMATION

Corresponding Author

*E-mail: sanyuanchen@mail.nctu.edu.tw. Tel: 8863-5731818. Fax: 8863-5724727.

Notes

The authors declare no competing financial interest.

ACKNOWLEDGMENTS

The authors gratefully acknowledge the financial support of the National Science Council of Taiwan through Contract 102-2221-E-009-043-MY3 and MOST 104-3113-E-042A-001.

DOI: 10.1021/acsami.5b00033
ACS Appl. Mater. Interfaces 2015, 7, 6172−6179

REFERENCES

(1) Yang, Y. P.; Zhai, R. R.; Duan, L. Q.; Masoud, K.; Kumar, P.; John, O. Integration and evaluation of a power plant with a CaO-based CO_2 capture system. *Int. J. Greenhouse Gas Control* **2010**, *4*, 603−612.

(2) Rochelle, G. T. Amine scrubbing for CO_2 capture. *Science* **2009**, *325*, 1652−1654.

(3) Liebenthal, U.; Pinto, D. D. D.; Monteiro, J. G. M. S.; Svendsen, H. F.; Kather, A. Overall process analysis and optimization for CO_2 capture from coal fired power plants based on phase change solvents forming two liquid phases. *Energy Proc.* **2013**, *37*, 1844−1854.

(4) Li, J. R.; Ma, Y. G.; McCarthy, M. C.; Sculley, J.; Yu, J. M.; Jeong, H. K.; Balbuena, P. B.; Zhou, H. C. Carbon dioxide capture-related gas adsorption and separation in metal-organic frameworks. *Coord. Chem. Rev.* **2011**, *255*, 1791−1823.

(5) Mavroudi, M.; Kaldis, S. P.; Sakellaropoulos, G. P. Reduction of CO_2 emissions by a membrane contacting process. *Fuel* **2003**, *82*, 2153−2159.

(6) D'Allesandro, D. M.; Smit, B.; Long, J. R. Carbon dioxide capture: prospects for new materials. *Angew. Chem., Int. Ed.* **2010**, *49*, 6058−6082.

(7) Siriwardane, R. V.; Shen, M. S.; Fisher, E. P.; Poston, J. A. Adsorption of CO_2 on molecular sieves and activated carbon. *Energy Fuels* **2001**, *15*, 279−284.

(8) Xu, P.; Xie, M. M.; Cheng, Z. M.; Zhou, Z. M. CO_2 capture performance of CaO-based sorbents prepared by a sol−gel method. *Ind. Eng. Chem. Res.* **2013**, *52*, 12161−12169.

(9) Valverde, J. M. Ca-based synthetic materials with enhanced CO_2 capture efficiency. *J. Mater. Chem. A* **2013**, *1*, 447−468.

(10) Plank, J.; Hoffmann, H.; Schölkopf, J.; Seidl, W.; Zeitler, I.; Zhang, Z. Preparation and Characterization of a Calcium Carbonate Aerogel. *Res. Lett. Mater. Sci.* **2009**, DOI: 10.1155/2009/138476.

(11) Wang, X. Y.; Alvarado, V.; Swoboda-Colberg, N.; Kaszuba, J. P. Reactivity of dolomite in water-saturated supercritical carbon dioxide: Significance for carbon capture and storage and for enhanced oil and gas recovery. *Energy Conversion Manage.* **2013**, *65*, 564−573.

(12) Rau, G. H. Electrochemical CO_2 Capture and Storage with Hydrogen Generation. *Energy Proc.* **2009**, *1*, 823−828.

(13) Yin, H. Y.; Mao, X. H.; Tang, D. Y.; Xiao, W.; Xing, L. R.; Zhu, H.; Wang, D. H.; Sadoway, D. R. Capture and electrochemical conversion of CO_2 to value-added carbon and oxygen by molten salt electrolysis. *Energy Environ. Sci.* **2013**, *6*, 1538−1545.

(14) Michael, C.; Stern, M. C.; Simeon, F.; Herzogb, H.; Alan Hatton, T. Post-combustion carbon dioxide capture using electrochemically mediated amine regeneration. *Energy Environ. Sci.* **2013**, *6*, 2505−2517.

(15) Blamey, J.; Anthony, E. J.; Wang, J.; Fennell, P. S. The calcium looping cycle for large-scale CO_2 capture. *Prog. Energy Combust. Sci.* **2010**, *36*, 260−279.

(16) Anthony, E. J. Ca looping technology: current status, developments and future directions. *Greenhouse Gas. Sci. Technol.* **2011**, *1*, 36−47.

(17) Yu, F. C.; Phalak, N.; Sun, Z. C.; Fan, L. S. Activation strategies for calcium-based sorbents for CO_2 capture: a perspective. *Ind. Eng. Chem. Res.* **2012**, *51*, 2133−2142.

(18) Liu, W. Q.; An, H.; Qin, C. L.; Yin, J. J.; Wang, G. X.; Feng, B.; Xu, M. H. Performance enhancement of calcium oxide sorbents for cyclic CO_2 capture-a review. *Energy Fuels* **2012**, *26*, 2751−2767.

(19) Kierzkowska, A. M.; Pacciani, R.; Müller, C. R. CaO-based CO_2 sorbents: from fundamentals to the development of new, highly effective materials. *ChemSusChem.* **2013**, *6*, 1130−1148.

(20) Li, Z. S.; Liu, Y.; Cai, N. S. Understanding the effect of inert support on the reactivity stabilization for synthetic calcium based sorbents. *Chem. Eng. Sci.* **2013**, *89*, 235−243.

(21) Li, Z. S.; Cai, N. S.; Huang, Y. Y.; Han, H. J. Synthesis, experimental studies, and analysis of a new calcium-based carbon dioxide absorbent. *Energy Fuels.* **2005**, *19*, 1447−1452.

(22) Li, Z. S.; Cai, N. S.; Huang, Y. Y. Effect of preparation temperature on cyclic CO_2 capture and multiple carbonation-calcination cycles for a new Ca-based CO_2 sorbent. *Ind. Eng. Chem. Res.* **2006**, *45*, 1911−1917.

(23) Martavaltzi, C. S.; Lemonidou, A. A. Development of new CaO based sorbent materials for CO_2 removal at high temperature. *Microporous Mesoporous Mater.* **2008**, *110*, 119−127.

(24) Martavaltzi, C. S.; Lemonidou, A. A. Parametric study of the CaO-$Ca_{12}Al_{14}O_{33}$ synthesis with respect to high CO_2 sorption capacity and stability on multicycle operation. *Ind. Eng. Chem. Res.* **2008**, *47*, 9537−9543.

(25) Xu, P.; Xie, M. M.; Cheng, Z. M.; Zhou, Z. M. CO_2 Capture Performance of CaO-Based Sorbents Prepared by a Sol−Gel Method. *Ind. Eng. Chem. Res.* **2013**, *52*, 12161−12169.

(26) Zhang, M.; Peng, Y. X.; Sun, Y. Z.; Li, P.; Yu, J. G. Preparation of CaO−Al_2O_3 sorbent and CO_2 capture performance at high temperature. *Fuel.* **2013**, *111*, 636−642.

(27) Florin, N. H.; Blamey, J.; Fennell, P. S. Synthetic CaO-Based Sorbent for CO_2 Capture from Large-Point Sources. *Energy Fuels* **2010**, *24*, 4598−4604.

(28) Liu, Y. M.; Tsunoyama, H.; Akita, T.; Tsukuda, T. Preparation of ∼1 nm Gold Clusters Confined within Mesoporous Silica and Microwave-Assisted Catalytic Application for Alcohol Oxidation. *J. Phys. Chem. C* **2009**, *113*, 13457−13461.

(29) Newalkar, B. L.; Olanrewaju, J.; Komarneni, S. Direct synthesis of titanium-substituted mesoporous SBA-15 molecular sieve under microwave-hydrothermal conditions. *Chem. Mater.* **2001**, *13*, 552−557.

(30) Zhang, Z. R.; Pinnavaia, T. Mesostructured forms of the transition phases η- and χ-Al_2O_3. *Angew. Chem.* **2008**, *120*, 7611−7614.

(31) Yuan, Z. Y.; Su, B. L. Surfactant-assisted nanoparticle assembly of mesoporous b-FeOOH (akaganeite). *Chem. Phys. Lett.* **2003**, *381*, 710−714.

(32) Ren, T. Z.; Yuan, Z. Y.; Su, B. L. Surfactant-assisted preparation of hollow microspheres of mesoporous TiO_2. *Chem. Phys. Lett.* **2003**, *374*, 170−175.

(33) Colomban, P. Raman study of the formation of transition alumina single crystal from protonic β/β'' aluminas. *J. Mater. Sci. Lett.* **1988**, *7*, 1324−1326.

(34) Priya, G. K.; Padmaja, P.; Warrier, K. G. K.; Damodaran, A. D.; Aruldhas, G. Dehydroxylation and high temperature phase formation in sol-gel boehmite characterized by Fourier transform infrared spectroscopy. *J. Mater. Sci. Lett.* **1997**, *16*, 1584−1587.

(35) Mercury, J.M. R.; Aza, A. H. D.; Turrillas, X.; Pena, P. The synthesis mechanism of $Ca_3Al_2O_6$ from soft mechanochemically activated precursors studied by time-resolved neutron diffraction up to 1000 °C. *J. Solid State Chem.* **2004**, *177*, 866−874.

(36) Gruene, P.; Belova, A. G.; Yegulalp, T. M.; Farrauto, R. J.; Castald, M. J. Dispersed calcium oxide as a reversible and efficient CO_2-sorbent at intermediate temperatures. *Ind. Eng. Chem. Res.* **2011**, *50*, 4042−4049.

(37) Lysikov, A. I.; Salanov, A. N.; Okunev, A. G. Change of CO_2 carrying capacity of CaO in isothermal recarbonation-decomposition cycles. *Ind. Eng. Chem. Res.* **2007**, *46*, 4633−4638.

DOI: 10.1021/acsami.5b00033
ACS Appl. Mater. Interfaces 2015, 7, 6172−6179